JGR Oceans

RESEARCH ARTICLE
10.1029/2019JC015167

Key Points:
- The speciation of Mn in the water column of four continental shelf sites was dominated by soluble Mn(III)-ligand complexes
- Over a diel cycle, Mn speciation shifted dramatically in both the photic and aphotic zone; total Mn changing by 100 nM in just a few hours
- Mn speciation varied spatially and temporally, the combined result of light, mixing and terrestrial inputs, as well as biological cycling

Correspondence to:
V. E. Oldham and C. M. Hansel,
voldham@uri.edu;
chansel@whoi.edu

Citation:
Oldham, V. E., Lamborg, C. H., & Hansel, C. M. (2020). The spatial and temporal variability of Mn speciation in the coastal Northwest Atlantic Ocean. *Journal of Geophysical Research: Oceans*, *125*, e2019JC015167. https://doi.org/10.1029/2019JC015167

Received 25 MAR 2019
Accepted 3 DEC 2019
Accepted article online 20 DEC 2019

The Spatial and Temporal Variability of Mn Speciation in the Coastal Northwest Atlantic Ocean

V. E. Oldham[1,3], C. H. Lamborg[2], and C. M. Hansel[1]

[1]Department of Marine Chemistry and Geochemistry, Woods Hole Oceanographic Institution, Woods Hole, MA, USA, [2]Department of Ocean Sciences, University of California, Santa Cruz, CA, USA, [3]Now at Graduate School of Oceanography, University of Rhode Island, Narragansett, RI, USA

Abstract Manganese (Mn) is distributed widely throughout the global ocean, where it cycles between three oxidation states that each play important biogeochemical roles. The speciation of Mn in seawater was previously operationally defined on filtration, with soluble Mn presumed to be Mn(II) and solid-phase Mn as Mn(III/IV) oxides. Recent findings of abundant soluble Mn(III) complexes (Mn(III)-L) highlights the need to reexamine the redox cycling of Mn, as these complexes can donate or accept electrons. To better understand the complex cycling of Mn in coastal waters, the distribution of Mn species at four Northwest Atlantic sites with different characteristics was examined. Diurnal influences on Mn speciation were investigated within a productive site. At all sites, Mn(III)-L complexes dominated, particularly in surface waters, and Mn oxides were low in abundance in surface waters but high in bottom waters. Despite intrasite similarities, Mn speciation was highly variable between our stations, emphasizing the diverse processes that impact Mn redox. Diel Mn measurements revealed that the cycling of Mn is also highly variable over time, even on time scales as short as hours. We observed a change of over 100 nM total Mn over 17 hrs and find that speciation changed drastically. These changes could include contributions from biological, light-mediated, and/or abiotic mechanisms but more likely point to the importance of lateral mixing at coastal sites. This exploration demonstrates the spatial and temporal variability of the Mn redox cycle and indicates that single timepoint vertical profiling is not sufficient when describing the geochemistry of dynamic coastal systems.

Plain Language Summary Manganese (Mn) is an essential micronutrient in seawater and an important player in the reactions of many other biologically relevant elements. The role of Mn in seawater is governed by its speciation: oxidation state (+2 to +4 in natural systems) and coordination environment. Manganese speciation is dominated by three species: soluble Mn(II), soluble Mn(III)-ligand complexes, and solid Mn oxides. Most studies of Mn in seawater focus only on solid versus soluble phase speciation, but this does not adequately describe the redox cycling of Mn because each species has unique chemistry in seawater. Here, we add to the limited studies that examine the speciation of Mn in seawater and find that Mn(III)-ligand complexes dominate our four coastal sites. This is important because Mn(III) can donate or accept electrons, making it particularly reactive and versatile. The complex cycle of Mn in coastal waters is dominated by each site's unique biology, the light regime, and water mixing processes. In addition, we examine the speciation of Mn over a diel cycle and find that Mn speciation changes dramatically from day to night, likely a mixing response. Thus, we find that the cycling of Mn is more variable over space and time than previously thought.

1. Introduction

Manganese (Mn) is an essential micronutrient, including in seawater, where it serves as a redox mediator and cofactor in enzymes necessary for photosynthesis, antioxidant activity, and other physiological processes (Hansel et al., 2017; Geszvain et al., 2013). Manganese is also a potent redox reactant within the environment and participates in the cycling of other bioactive elements including carbon (C), nitrogen (N), oxygen (O), sulfur (S), and iron (Fe), to name a few (Tebo et al, 2004; Hansel & Learman, 2015). Reduced and soluble Mn(II) is an important scavenger of the reactive oxygen species (ROS) superoxide ($O_2^{\bullet-}$; Wuttig et al., 2013; Hansard et al., 2011), leading to the formation of oxidized Mn (Learman et al., 2011; 2013). Oxidized forms of Mn(aqueous Mn(III)-ligand complexes and Mn(III/IV) oxides) are among the strongest oxidants in seawater after O_2 (Luther, 2005), and solid-phase Mn(III/IV) oxides also have high sorption capacities, garnering them a reputation as "scavengers of the sea" (Goldberg, 1954).

A major impediment to a greater understanding of the redox cycling of Mn in the ocean is the lack of understanding of its speciation beyond the phase (dissolved vs. particle) distinction. While there is a fair amount of data regarding total and dissolved Mn, this is not enough to address the impact that Mn has on other biogeochemical cycles because the reactivity of Mn varies with oxidation state. Until recently, the speciation of Mn was operationally defined by filtration, where the fraction that passed through a 0.2-μm filter was presumed to be soluble Mn(II), and the fraction retained on the filter was considered solid-phase Mn(III/IV) oxides (predominantly thought to be as Mn(IV)) (see, e.g., Graham et al., 1976). The oxidation of Mn(II) to Mn(IV) oxides, however, occurs via two, separate, one-electron transfer steps, as the donating and accepting molecular orbitals between Mn(II) and Mn(IV) are spatially distinct (Luther, 2005). Mn(III), therefore, is formed as an intermediate. Although aqueous Mn(III) disproportionates rapidly at pH < 7, at seawater pH and in the presence of suitable ligands (L), this Mn(III) intermediate forms Mn(III)-L complexes instead. In fact, these Mn(III)-L complexes have recently been shown to be a dominant component of dissolved Mn within estuaries and ocean basins (Trouwborst et al., 2006; Dellwig et al., 2012; Yakushev et al., 2009; Madison et al., 2011, 2013; Oldham et al., 2015, 2017a,b,c). Additionally, Mn(III) has been shown to bind to the same ligands as Fe(III) (Duckworth & Sposito, 2005, 2007; Parker et al., 2007) with stability constants similar to or exceeding those of analogous Fe(III)-L complexes (Luther et al., 2015). Thus, Mn(III)-L complexes are now considered to be an important part of the Mn pool and may be a particularly reactive fraction as they can both donate and accept electrons. Previous studies, which have only considered solid versus soluble Mn, therefore, do not fully account for the full redox capacity of Mn.

At seawater pH, the thermodynamically favored state of Mn is Mn(IV), present as oxy (hydr)oxide solid phases (Morgan, 2005). Nevertheless, soluble Mn is abundant and stable in the marine waters (up to 12 μM, Trouwborst et al., 2006). In fact, unlike most transition metals, soluble Mn actually exhibits a surface maximum (Landing and Bruland, 1980). This distribution is due in part to thermodynamic and kinetic constraints on abiotic Mn(II) oxidation to Mn(III) by O_2 (Luther, 2005) but may be better explained by inorganic and organic reductive processes, many of which are sunlight-induced reactions. Specifically, most soluble Mn in the surface ocean is thought to persist due to photo-assisted reductive dissolution of Mn oxides (e.g., Sunda et al., 1983) and/or light inhibition of microbial Mn(II) oxidation (Sunda & Huntsman, 1988). The sunlight-induced production of ROS like superoxide ($O_2^{\bullet-}$) and hydrogen peroxide (H_2O_2) may also be an important mechanism in controlling both the formation and reductive dissolution of Mn oxides. Both of these ROS are major photochemical products in seawater, with superoxide concentrations in sunlit waters up to 10 nM (Petasne and Zika, 1987; Rose et al., 2008, 2010) and H_2O_2 persisting longer with concentrations in the range of 10–200 nM (Cooper et al., 1988). Further, extracellular production of both superoxide and hydrogen peroxide by marine phytoplankton and bacteria is now known to be widespread and a major source of ROS within both dark and sunlit waters (e.g., Diaz et al., 2013; Hansel et al., 2016; Marshall et al., 2005; Rose et al., 2010; Schneider et al., 2016). Superoxide is an oxidant of Mn(II) (Hansard et al., 2011; Wuttig et al., 2013), and both photochemical and biological superoxide production have been linked to Mn oxidation and oxide formation (Hansel et al., 2012; Learman et al., 2011; Nico et al., 2002). On the other hand, H_2O_2 is a reductant of oxidized Mn species (Baral et al., 1985; Learman et al., 2013). Thus, ROS can lead to the formation of Mn(III)-L via both oxidative and reductive pathways.

Below the photic zone, in the absence of light-associated reductive processes, dark oxidative processes lead to the formation of Mn oxides. For example, the surface-catalyzed oxidation of Mn(II) occurs on metal oxide surfaces, either autocatalytically (e.g., Mn(II) on MnOOH; Morgan, 2005) or on other metal oxides (e.g., Mn(II) on Fe oxides; Wehrli, 1990; Madden & Hochella, 2005). Further, a wide diversity of bacteria (Tebo et al., 2004; Hansel, 2017) oxidize Mn(II) via direct enzymatic activity involving either multicopper oxidases (Gezvain et al., 2013) or animal heme peroxidases (Anderson et al., 2009). Mn(III) is produced as an intermediate (Webb et al., 2005; Dick et al., 2008; Johnson & Tebo, 2008), which is bound reversibly to the enzyme site that oxidized the Mn(II) and can therefore either be stabilized by ligands or get further oxidized to Mn oxides (Butterfield et al., 2013). In addition to direct microbial oxidation, microbial production of extracellular superoxide-producing enzymes leads to the oxidation of Mn(II) to Mn(III) (Learman et al., 2011; Learman & Hansel, 2014) and ultimate formation of Mn oxides within both sunlit and dark conditions (Learman et al., 2011; Andeer et al., 2015). Thus, both the direct and indirect microbial oxidation of Mn(II) may act as a source of Mn(III)-L to seawater.

Additionally, the dissolution of Mn oxides by ligand-promoted reductive dissolution can also be achieved in the absence of light, with Mn(III)-L as a product (Duckworth & Sposito, 2007; Oldham et al., 2015). This may be a particularly favorable mechanism for the formation of Mn(III)-L complexes in the presence of dissolved organic carbon (Stone, 1987a, 1987b; Stone & Morgan, 1984). Laboratory experiments indicate that ligand-promoted oxidation of Mn(II) by the Mn(III)-binding ligand desferrioxamine-B is possible with O_2 as the oxidant (Duckworth & Sposito, 2005), but there are no direct studies of Mn(II) oxidation by natural organic matter leading to the formation of Mn(III)-L.

The reactions surrounding the redox cycle of Mn in coastal systems are complex, with many oxidative and reductive pathways co-occurring, particularly in surface waters and shallow water column sites (<100 m) where the influence of light, ROS, particles, and biology interact. Here, we sought to expand our understanding of the redox cycling of Mn in coastal systems, beyond estuaries and stratified ocean basins. To do so, we profiled the speciation of Mn at four biogeochemically distinct coastal sites in the Northwest Atlantic off the east coast of the United States in August 2017 (Figure 1). To fully incorporate the influence of diurnal changes in light, ROS, and microbial activity, we also examined Mn speciation at a highly productive coastal site off the coast of New Jersey over a diel cycle. This exploration further highlights the dominance of Mn(III)-L complexes and demonstrates the variability and complexity of the Mn redox cycle within coastal systems.

2. Materials and Methods

2.1. Sample Collection

Samples were collected from four water column sites along the northeast coast of the United States (Figure 1) in August 2017 aboard the R/V Endeavor. Samples for Mn speciation were collected using a paint-sealed Sea-Bird rosette, outfitted with a Sea-Bird SBE 19 Plus V2 recording CTD (conductivity, temperature, and depth) and 8-L X-Niskins (General Oceanics). The Niskins were acid-cleaned in the laboratory prior to use and "pre-soaked" for 12 hr with local seawater collected at a shakedown station prior to deployment at the stations listed here. This "clean rosette" was lowered on a nonmetallic line (1/4" O.D. vinyl-jacketed Vectran) and bottle closure at preprogrammed depths controlled by a Sea-Bird Auto-firing Module. Sample depths were chosen based on the real-time water column profile data obtained from the ship's CTD rosette system (Sea-Bird) that was deployed before the "clean rosette" and which also provided the dissolved oxygen, salinity, PAR (Photosynthetically Active Radiation), beam transmission, and fluorescence profiles reported here. Site-specific depths were chosen to target the surface, the chlorophyll maximum, the top of the aphotic zone, the center of the aphotic zone, and the 3 m off above the sediment-water interface. Immediately following recovery of the "clean rosette," the Niskins were removed from the frame and moved to a shipboard HEPA (High-Efficiency Particulate Air) - filled "bubble," where samples were immediately decanted through acid-washed C-flex silicone tubing directly into acid-washed 1-L PTFE (Polytetrafluoroethylene) bottles. Samples were kept refrigerated and in the dark until analysis and were analyzed within 2 hrs of collection.

2.2. Mn Measurements

Seawater samples (1 L) were filtered through 0.2-μm membrane filters (Millipore) within 1 hr of collection using acid-washed Savillex vacuum-filtration rigs. The filtrate was poured into new 15-ml Falcon tubes, and the filter was immediately amended with a leuco-based dye for Mn oxide concentration determination in a separate 15 ml Falcon tube.

The leucoberbelin blue (LBB) assay for Mn oxides (denoted MnOx hereafter) was previously adapted from Altmann (1972) to examine coastal water column sites (Oldham et al., 2015; Oldham et al., 2017; Oldham et al., 2017; Oldham et al., 2017). In this assay, the filter is amended with 3 ml of 20-μM LBB dye solution (LBB, Sigma-Aldrich). The dye color forms upon oxidation of the LBB molecule by Mn oxides and can be measured spectrophotometrically. The LBB stock solution was prepared by dissolving the powder in Milli-Q water to a concentration of 4% and adding 40 μl of 10 M sodium hydroxide (NaOH) per 10 ml of stock solution. Working solutions are subsequently prepared by diluting the stock solution into 1% acetic acid (v/v), to 0.4% LBB. A calibration curve was generated using $KMnO_4$, for which equivalent absorbance for Mn(IV) is calculated based on 2.5 more Mn(IV) being required relative to Mn(VII) to oxidize the LBB. In our setup, a 100-cm pathlength cell (Liquid Waveguide Capillary Cell) was coupled to a flame UV-Vis (Ocean Optics), set up with SpectraSuite software. Using a 100-cm pathlength cell allows for a detection limit of 0.05 nM but also

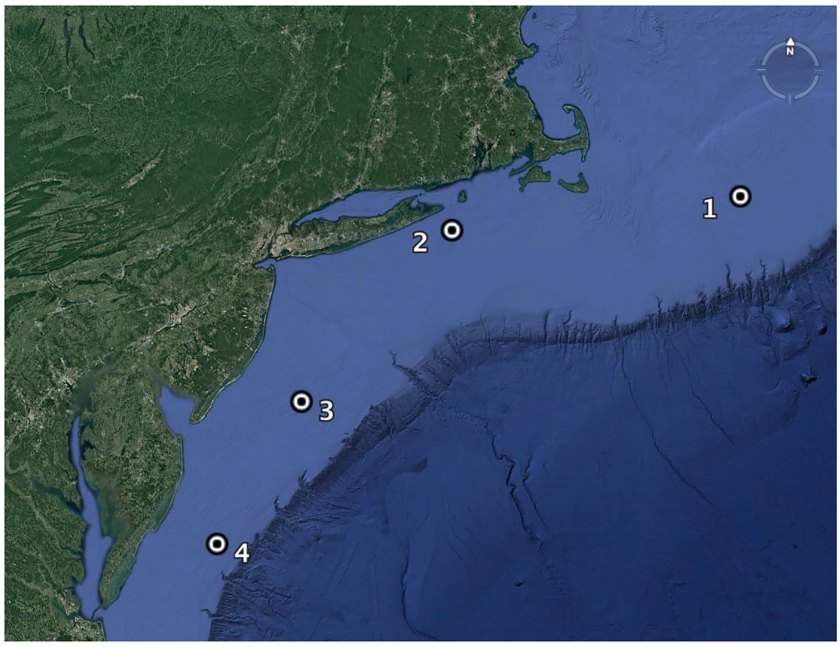

Figure 1. Station map for the four stations explored in this study, Station 1 at Georges Bank (41.18026, −67.92692), Station 2 near Block Island (40.8722, −71.69217), Station 3 off the New Jersey coast (39.18884, −73.56232), and Station 4 off the Maryland coast (37.77692, −74.56461).

requires our refiltration of samples (0.2-μm luer-lok syringe filter, Millipore) prior to injection into the cell to avoid particulate interference and clogging of the capillary cell. Previous work using this methodology has reported an error of <2%. Samples reacted with the LBB dye overnight in the dark prior to analysis, then absorbance at 623 nm was recorded. If sample absorbance was too high, samples were diluted 10–20 times in Milli-Q water.

For soluble Mn speciation analysis, an established spectrophotometric porphyrin addition method was employed (Madison et al., 2011; Oldham, Mucci, et al., 2017), which uses the ligand T(4-CP)P (or α, β, γ, δ-tetrakis(4-carboxyphenyl)porphine, to 2.33×10^{-7} M final sample concentration). In this method, cadmium chloride ($CdCl_2$; to 2.4×10^{-7} M) is added to form a complex with the porphyrin, in the presence of an imidazole tetraborate buffer (pH = 8.2). The sample is added to the mixture (diluted 10-fold with Milli-Q water to avoid chloride interference) and any Mn(II) in the sample undergoes a metal substitution reaction with the Cd over the course of a 1-hr reaction in a 90°C water bath. The solution is cooled, then analyzed using the 100-cm UV-Vis spectrophotometric setup described above. Total dissolved Mn is analyzed in the same way but after the addition of 1.4 μM hydroxylamine hydrochloride to the sample (reacted overnight in a refrigerator). The difference between the total dissolved Mn and the Mn(II) gives the Mn(III)-L in the sample. We note that during the heated reaction with no reducing agent, it is likely that some Mn(III)-L complexes undergo a ligand substitution reaction with the added porphyrin, and thus our method likely underestimates Mn(III)-L, particularly for weaker complexes. For all samples, assays were run in triplicate for both Mn(II) and Mn total, and peak height for all assays was determined using a baseline subtraction performed using ECD-Soft peak correction software.

3. Results

Here we provide data from four biogeochemically distinct sites that each capture different aspects of coastal Mn redox chemistry (Figure 2, Table 1). The results herein focus first on the water column profiles of four stations, followed by the results from a diel cycle at Station 3 (New Jersey Shore; Figures 3–4).

3.1. Mn Speciation with Depth

3.1.1. Station 1—Georges Bank

Station 1, Georges Bank, was the northmost site in this study and the furthest from shore. It was a well-mixed site, as indicated by the vertically uniform dO_2, temperature, and salinity profiles in Figure 2 (Top, Panel D).

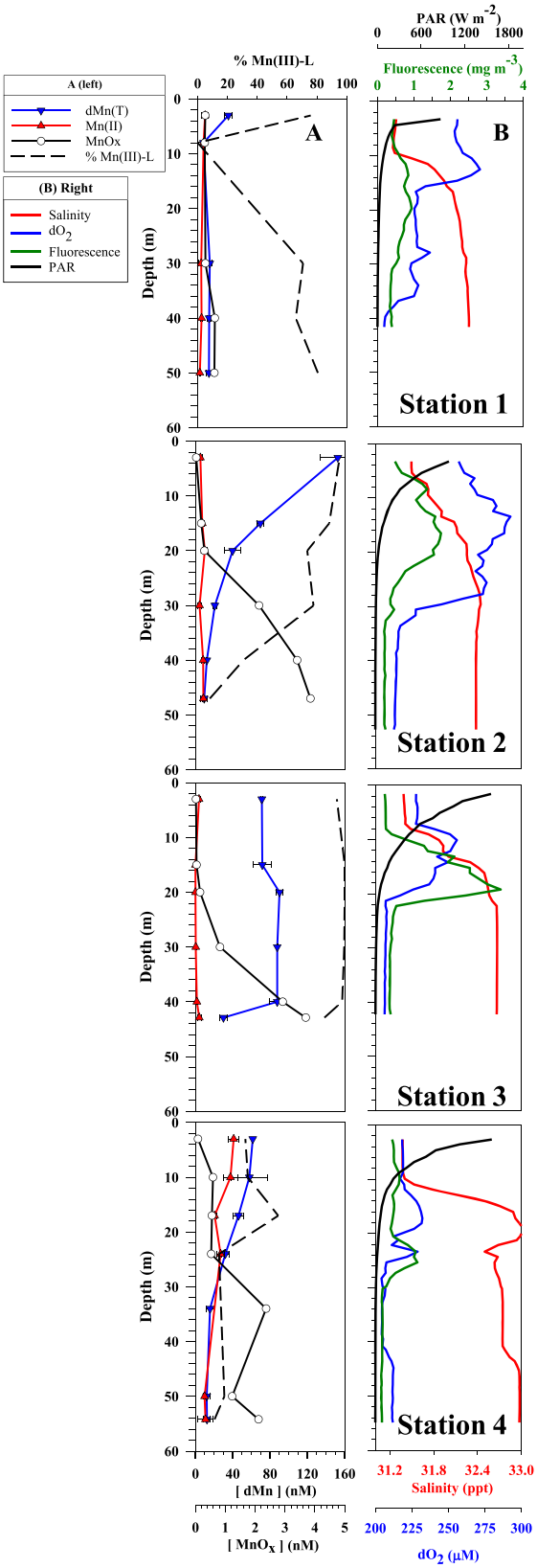

Figure 2. Speciation profiles for Mn (a) and water column physicochemical properties (b) for four stations (starred on maps) moving north to south from top to bottom.

Table 1
Physicochemical Data Collected From the CTD Rosette Package and Mn Speciation (in nM).

Station	Depth (m)	Temperature (°C)	Salinity (ppt)	Fluorescence (mg m^{-3})	PAR (μE m^{-2} s^{-1})	% Beam transmission	dO2 (μM)	Mn (II)	dMnT	Mn (III)-L	% Mn (III)-L	MnOx
Station 1 Georges Bank	3	16.22	32.25	0.94	1,195.8	74.9	265.2	9.94 ± 2.39	33.02 ± 3.75	23.08 ± 4.45	69.90	0.26
	8	16.29	32.25	1.66	395.4	75.3	264.4	6.34 ± 0.54	6.19 ± 0.08	0.00 ± 0.55	0.00	0.24
	30	16.10	32.25	1.81	2.3	75.1	262.5	3.80 ± 3.20	12.96 ± 2.20	9.16 ± 3.88	70.70	0.26
	40	15.98	32.26	1.97	0.2	74.9	261.9	4.24 ± 1.40	12.38 ± 2.19	8.14 ± 2.60	65.76	0.58
	50	15.92	32.26	1.89	0.0	71.9	261.6	2.36 ± 0.54	12.15 ± 3.10	9.79 ± 3.15	80.61	0.56
Station 2 Block Island	3	21.61	31.49	0.54	1,008.4	76.3	257.1	5.20 ± 1.90	152.70 ± 18.73	147.49 ± 18.83	96.59	ND
	15	15.23	32.08	1.60	122.1	76.8	289.9	7.21 ± 2.58	69.53 ± 3.13	62.32 ± 4.06	89.63	0.19
	20	14.05	32.26	1.58	44.6	77.6	276.5	9.99 ± 2.73	44.93 ± 0.59	34.94 ± 2.79	77.77	0.30
	30	10.61	32.44	0.42	8.8	82.6	245.3	4.35 ± 1.68	20.80 ± 2.02	16.44 ± 2.63	79.07	2.13
	40	9.39	32.38	0.25	2.3	78.8	214.6	8.21 ± 1.34	12.08 ± 0.32	3.87 ± 1.38	32.05	3.41
	47	9.36	32.38	0.24	0.7	78.5	213.7	8.42 ± 0.76	9.31 ± 3.66	0.89 ± 3.74	9.56	3.85
Station 3 New Jersey Shore	3	24.94	31.39	0.26	1,323.9	82.1	258.0	3.77 ± 1.27	71.17 ± 1.02	67.40 ± 1.63	94.70	ND
	15	13.09	32.30	1.98	189.8	73.9	249.7	0.00 ± 0.00	77.48 ± 0.23	77.48 ± 0.23	100.00	ND
	20	10.68	32.55	3.43	65.3	75.7	226.0	0.00 ± 0.00	90.11 ± 3.46	90.11 ± 3.46	100.00	0.15
	30	9.56	32.67	0.43	12.2	81.7	207.0	0.30 ± 1.06	87.60 ± 0.52	87.31 ± 1.18	99.66	0.82
	40	9.56	32.66	0.39	3.3	81.6	206.5	1.51 ± 0.67	87.65 ± 7.97	86.14 ± 8.00	98.28	2.92
	42.9	9.56	32.66	0.39	2.4	81.6	206.5	4.07 ± 1.91	29.99 ± 3.83	25.92 ± 4.28	86.42	3.70
Station 4 Maryland Shore	3	25.75	31.37	0.46	1,595.0	75.8	218.4	40.90 ± 5.52	61.41±	20.51 ± 5.52	33.39	0.08
	10	25.68	31.40	0.66	248.8	76.5	216.9	37.46 ± 7.55	68.82 ± 2.18	31.36 ± 7.86	45.57	0.59
	17	22.69	32.92	0.48	67.6	83.2	232.2	20.55 ± 2.38	46.09 ± 5.45	25.54 ± 5.95	55.41	0.55
	24	14.15	32.68	1.06	25.2	81.1	221.6	26.91 ± 4.41	31.93 ± 4.14	5.02 ± 6.05	15.73	0.53
	34	9.73	32.74	0.20	4.4	84.5	204.6	0.00±	15.57 ± 4.17	15.57 ± 4.17	100.00	2.37
	50	8.62	32.98	0.16	0.5	84.0	212.0	9.74 ± 1.10	12.07 ± 3.71	2.33 ± 3.87	19.33	1.23
	54.2	8.62	32.97	0.18	0.3	84.0	211.6	14.77 ± 5.42	12.25 ± 3.84	0.00 ± 6.64	0.00	2.11

Note. Blank spaces indicate samples where no data was collected. Blank standard deviations represent where $n = 1$, and ND reflects values below the detection limit.

The PAR was attenuated to <1% by 20 m in the water column, below which there was consistently high fluorescence to depth. This contrasts with our other three stations, where there was a distinct chlorophyll maximum.

Of all four sites, Station 1 had the lowest concentrations of total dissolved Mn (dMn_T = 6–34 nM), with the majority of soluble Mn in the form of Mn(III)-L complexes (up to 80%) and highest concentrations of dMn_T in surface waters. Below the surface, at the top of the chlorophyll maximum (8 m, 1.66 mg m^{-3} of

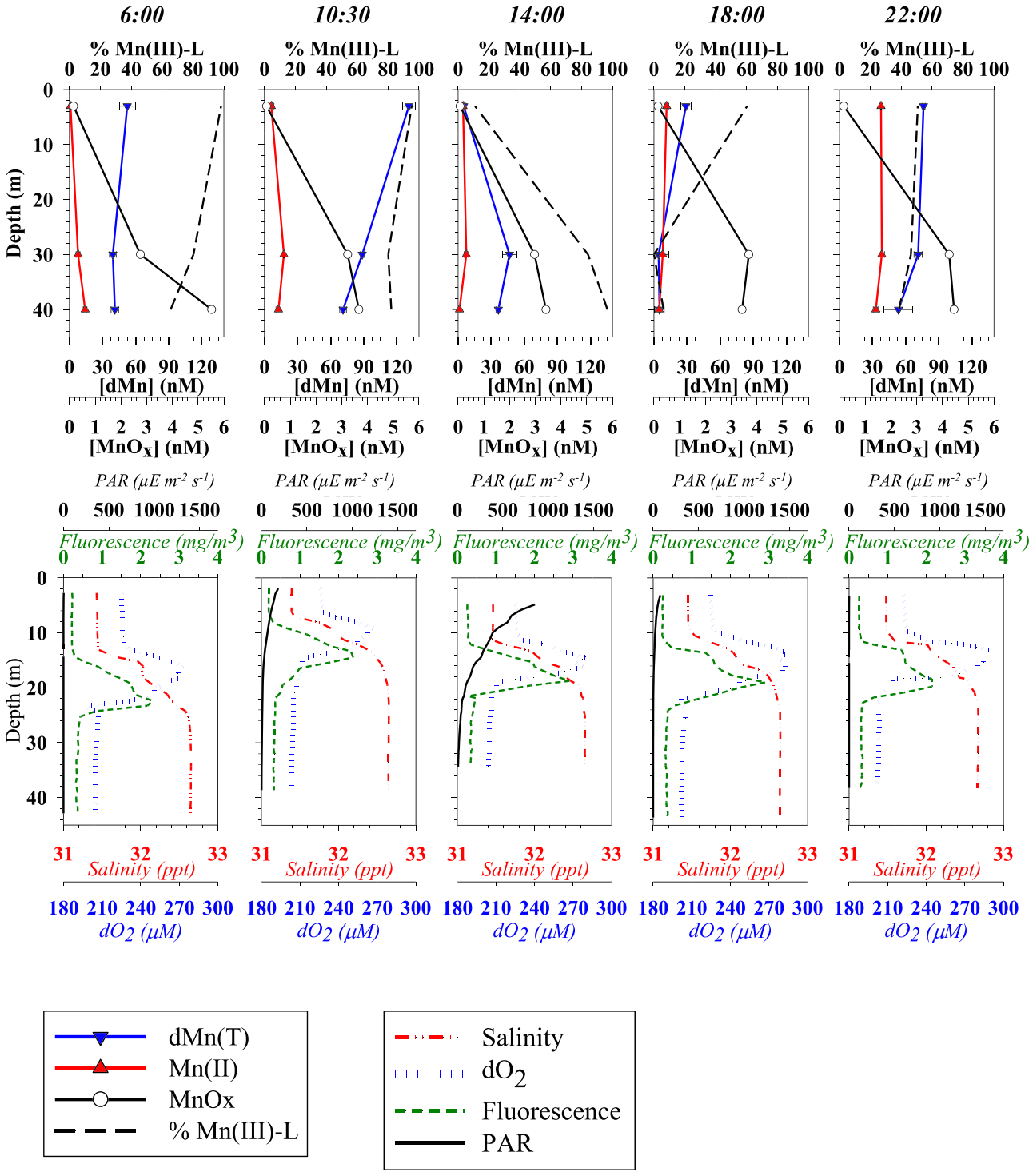

Figure 3. The speciation of Mn (top) and water column parameters (bottom: fluorescence, PAR, % beam transmission and dO_2) over the course of the diel cycle at Station 3 (New Jersey Shore). Error bars represent standard deviations of triplicate measurements for dissolved Mn.

fluorescence), we observed the lowest dMn_T (3.80 ± 3.20 nM), which was comprised entirely of Mn(II) (Figure 2, Panel A). The bottom three depths sampled had near constant dMn_T concentrations (~12 nM, 80% Mn(III)-L). MnO_x concentrations at this site were low in the top 30 m (0.24–0.26 nM) and doubled in the bottom 20-m depths (0.56–0.58 nM).

3.1.2. Station 2—Block Island

Station 2, near Block Island, exhibited more variability in the salinity and fluorescence profiles compared to Station 1, likely leading to more defined structure in the dissolved oxygen (dO_2) profile, which had a ~20 m thick maximum from 10- to 30-m depth. However, the vertical structure in the temperature profile suggests that this was still a fairly well-mixed site, and thus oxygen dynamics were likely the result of biological activity and not mixing.

As Station 2 is near Block Island, it is the closest site to terrestrial sources of metals and organic matter, which is reflected in higher dMn_T (9–153 nM) concentrations. At this station, the highest dissolved Mn concentrations were in surface waters, and this dMn was 97% Mn(III)-L. The concentration of dMn_T decreased exponentially from surface to depth, and the relative percentage of Mn complexation within the dMn_T decreased to only 10% of the 9 nM dMn_T complexed in bottom waters. This corresponded to higher MnO_x concentrations (3.85 nM at 50 m, compared to 0.03 nM in surface waters).

3.1.3. Station 3—New Jersey Shore

Station 3, off the coast of New Jersey, was characterized by a sharp fluorescence maximum at 20-m depth and a more stratified water column compared to Stations 1 and 2. High temperature and low salinity in the top 10 m reflected freshwater inputs, with a zone of mixing between 10 and 25 m, and low salinity and high temperature in the bottom 25 m, below the fluorescence maximum. The fluorescence maximum was within the photic zone, where its base was marked by the top of the aphotic zone. The fluorescence in this maximum (3.43 mg m^{-3}) was the highest observed during the sampling campaign and co-occurred with a small increase in dO_2. The oxygen profile at this site was less structured than at the Block Island site (Station 2).

The speciation of dissolved Mn was the least varied at this site, despite the vertical stratification of the water column and high productivity. Total dMn was 70–90 nM at all depths, except in the very bottom where it decreased to 33 nM, and was slightly more reduced (87% Mn(III)-L compared to 95–100% complexation at shallower depths). Solid MnO_x increased from surface (0.02 nM) to bottom (3.85 nM), with high bottom water MnO_x associated with the lowest dMn_T.

3.1.4. Station 4—Maryland Shore

At Station 4, our southernmost station, we observed the most vertically stratified water column, with high temperature and low salinity in the top 10 m of the water column, and a sharp increase in salinity from 10 to 17 m, whereas temperature decreased more gradually from 10 to 30 m. This may indicate slow mixing. PAR attenuated at 22 m, and the chlorophyll maximum was below the photic zone (24 m, 1.06 mg m^{-3} of fluorescence). This station also had the lowest dissolved O_2 of our four sites, which may be the result of stratification and high respiration.

Dissolved Mn concentrations were higher in the photic zone (61–69 nM, top 10 m) and decreased to 12 nM in the bottom 10 m of the water column. The speciation of Mn was most variable at this station, with % Mn(III)-L ranging from 0 to 100%.The highest concentration of Mn(III)-L was in mid-waters (34 m) and lowest at the deepest depth. The concentration of Mn oxides was highest at this site, with the levels increasing below the photic zone. Interestingly, the dMn_T in the bottom waters of this station was completely Mn(II) (14.77 nM), yet Mn oxides were also relatively high in concentration (2.11 nM).

3.2. Mn Speciation Throughout a Diel Cycle

To address the importance of direct and indirect light reactions on Mn speciation, we performed a diel sampling study at Station 3 at the New Jersey Shore site (Figures 3 and 4), examining the speciation of Mn at three depths (photic = 3 m, Aphotic 1 = 30 m, and Aphotic 2 = 40 m) over the course of 16 hr.

In Figure 3, the physicochemical parameters in the bottom panels indicate shifts in water column properties of our five sampling timepoints, particularly, shifts in the location of the oxygen and fluorescence maximum. At the first timepoint, before the appearance of sunlight, the fluorescence maximum is at 23 m, and dO_2 is highest at 15-m depth. Salinity profiles indicate a fresher layer in the top 14 m. By 10:30 EST (Eastern Standard Time), there was a shoaling of the fresher layer to 6 m. Further, peak dO_2 and fluorescence were found at 8 and 15 m, respectively, indicative of shifts in microbial photosynthesis and respiration and/or water column mixing (or, less likely, a slight change in the ship's position). At the afternoon timepoint (14:00 EST), PAR was highest, attenuated at 30 m, and the fluorescence maximum intensified and

deepened to 20 m, corresponding to a slightly deeper salinity maximum (11 m) and dO_2 maximum. Finally, by 22:00 EST, PAR was zero at all depths, but there was again little shift in the position of either the fluorescence or dO_2 maxima, indicating that afternoon light had little effect on the position of the productivity maximum and/or that mixing was less significant in the afternoon.

The speciation of Mn changed dramatically over the course of the diel cycle (Figure 3). Over the course of the day, total Mn (MnO_x + dMn_T summed for all three depths) ranged from 58 nM at 18:00 EST to 289 nM at 10:30 EST, which is most obvious in Figure 3. The first sampling at 6:00 EST, before sunrise, and at all three depths, dMn_T was ~40 nM and predominantly in the form of Mn(III)-L (70–100%). Mn oxide concentrations were most elevated at the deepest depth (5.5 nM) and below 0.5 nM in the surface. By 10:30 EST, dMn_T more than doubled in concentration at all depths with the greatest increase in the surface, and Mn oxide concentrations did not change significantly, except in Aphotic 2 where concentrations decreased by ~2 nM. At 14:00, when PAR was highest, we expected to see the highest concentrations of dMn_T and lowest MnO_x, but we instead saw a dramatic decrease in dMn_T from 138 to 5 nM in surface waters and by ~30 nM at our aphotic depths, while MnO_x did not change significantly. By 18:00 EST, PAR decreased to near zero in the surface and zero below, which coincided with a small increase in Mn oxide concentrations. In both aphotic depths, the concentration of dissolved Mn was at a minimum at this time. Additionally, during this timepoint, we observed more Mn(II) relative to Mn(III)-L, particularly in the aphotic depths. Finally, at our last sampling event, 22:00 EST, PAR decreased to zero at all depths, and the concentrations of solid and soluble Mn returned to values similar to what was observed at our first sampling event, at 6:00 EST. One exception is that at all depths, Mn(II) concentrations are highest at this timepoint.

4. Discussion

Here, we show that Mn(III)-L complexes comprise the bulk of the total Mn (solid + soluble) at four biogeochemically distinct coastal stations, making up to 100% of the total dissolved Mn, and always significantly in excess of Mn oxide concentrations (aside from one bottom depth at Station 4). Previous water column measurements of Mn in the Northwest Atlantic have focused on open ocean measurements of total Mn (e.g., Yeats and Bewers, 1985; Statham and Burton, 1986), estuarine measurements of total Mn (Sundby et al., 1981; Yeats et al., 1979) and Mn speciation (Oldham et al., 2015; Oldham, Mucci, et al., 2017; Oldham, Tebo, et al., 2017), or measurements in estuarine tributaries for total Mn (Boyle et al., 1974; Eastman & Church, 1984; Graham et al., 1976; Moore et al., 1979; Sholkovitz, 1978) and Mn speciation (Oldham, Miller, et al., 2017). This study provides Mn(III)-L measurements and profiles along continental shelves and is one of only a handful of studies determining Mn speciation profiles in seawater.

The only nonestuarine shelf measurements of Mn in the Northwest Atlantic found that dMn_T concentrations were 21 nM in surface waters (Bruland & Franks, 1983) and previous estuarine measurements of Mn in Narragansett Bay, RI, near our Station 2 (Block Island) found elevated particulate Mn (pMn = 18–582 nM; Graham et al., 1976) and dMn_T (9–1,093 nM; Graham et al., 1976) relative to typical open ocean concentrations for dissolved Mn (0.1–3 nM; Landing and Bruland, 1980). Our measurements of dMn_T fall within the range of previous coastal measurements (9–153 nM), but we observe significantly lower MnO_x concentrations (<4 nM), which may be due to our selective assay for Mn oxides, where Graham et al. (1976) measured total pMn. However, it is more likely that our sites are far enough from the shore that most of the pMn precipitated via oxidative removal and adsorption processes along an increasing salinity gradient (Boyle et al., 1974).

The mechanisms expected to control the speciation and cycling of Mn observed at the four stations here are ultimately redox reactions, primarily driven by direct and indirect microbial activity. Thus, full interpretation of the controls on these species distributions would require detailed experimentation including incubations targeting chemical and biological redox reactions and controlled kinetic experiments. Nevertheless, examination of the spatial and temporal changes in Mn speciation within these biogeochemically distinct sites reveal other factors influencing the concentration of Mn and the underpinning redox transformations, in particular (1) light (2) terrestrial inputs to surface waters, (3) primary productivity, and (4) lateral mixing.

4.1. Spatial Variability in Mn Speciation

Light is a dominant control on Mn speciation (e.g., Sunda & Huntsman, 1988), particularly the dissolution of Mn oxide particles, as observed via both the depth profiles and diel cycling measurements (see section 4.2). This is reflected in our observation of low MnO_X in all our surface samples and an MnO_X maximum in the bottom waters at three of our four sites (Figures 2–4). This distribution could reflect the settling of these particles to depth but more likely points to photo-reductive dissolution of Mn oxides in surface waters and significant oxidation processes below the photic zone, as we do not see particle accumulation in the beam attenuation in the water column of our sites (Table 1). In Narragansett Bay, Graham et al. (1976) observed high dissolved Mn concentrations in bottom waters, corresponding with a flux of dissolved Mn from the sediments to overlying waters. This is consistent with coastal work in the St. Lawrence Estuary (Oldham, Mucci, et al., 2017) which showed that dissolved Mn concentrations were 10 times higher in bottom waters than in surface waters. Oldham, Mucci, et al. (2017) also observed high MnO_x at depth, corresponding to a flux of Mn(II), suggesting that oxidative processes likely dominate in bottom waters. At Station 4, we similarly observe elevated MnO_x concentrations at depth with soluble Mn entirely in the form of Mn(II), indicating that there is some mechanism oxidizing Mn(II) completely to Mn(IV), and either lack of Mn(III)-L formation or low complex stability.

At most of our study sites, we observe the highest dMn_T concentrations in surface waters pointing to the role of surface export from nearby estuarine mixing. In some instances, total Mn (particulate + dissolved) behaves conservatively during estuarine mixing, even while the partitioning between the dissolved and particulate phases was not conservative (e.g., Graham et al., 1976). Rather, dMn_T was lost to the particulate phase either through oxidation or adsorption upon increasing salinity (and pH; Boyle et al., 1974; Graham et al., 1976). However, the seasonality of estuarine mixing of dissolved Mn has recently been evaluated in the Broadkill River (DE), a tributary to the Delaware Bay (Oldham, Miller, et al., 2017). In the Broadkill study, dMn_T was not conservatively mixed, but instead, in the late summer and fall, dissolved Mn was exported from the Broadkill River, predominantly as Mn(III)-L complexes (up to 100% of total Mn), and in the winter and spring months, dissolved Mn was conservatively mixed and more reduced. Further, Mn(III)-L was closely associated with humic-type organic matter, providing an explanation for the seasonality of Mn mixing, in particular, when organic matter inputs are high, the Mn(III)-binding ligand pool is sufficiently in excess of dissolved Mn, presumably preventing complete oxidation to Mn oxides. Thus, given that our study takes place in the late summer (August 2017), we expect to see complexation of dissolved Mn in surface waters, particularly at nearshore sites due to high organic matter export. At three of four stations, the highest dMn_T is observed in the top 10 m of the water column, indicating that surface runoff is indeed likely a source of soluble Mn along the coast, and that this dMn_T is predominantly in the form of organic Mn(III)-L complexes.

The % Mn(III)-L within bottom waters is variable among our sites (Figure 2). The % Mn(III)-L is low at Stations 2 and 4, which may correspond with Mn(II) fluxing from sediments or high oxidation rates of Mn(III) to Mn oxides and subsequent settling. At Station 1, % Mn(III)-L is higher in bottom waters, which may be the result of mixing processes exceeding oxidation rates at this well-mixed site. Interestingly, the % Mn(III)-L varies in bottom waters over the course of a diel cycle (Figure 3), suggesting that lateral mixing influences the accumulation of Mn(III)-L complexes in bottom waters or that the oxidation of Mn(III) to Mn oxides is biologically regulated and variable in response to diel metabolic activity and gene expression.

Biological assimilation of dissolved Mn may also be an important feature of our profiles, given that lower dissolved Mn concentrations often coincide with the fluorescence maximum. In this study, Chl-*a* measurements were made in a few samples, and ranged from 0.0 to 3.2 μg/L. Based on typical phytoplankton values of Chl-*a* to carbon ratios of 3×10^{-4}, Mn to C ratio of 3×10^{-5} (for *Thalassiosira pseudonana* in waters containing 100 nM of Mn; Sunda and Huntsman, 1995, 1996), and using a median value of 1.6 μg/L Chl-*a* from our measurements, we find that biological uptake can only account for 0.175 nM of Mn loss, less than 1% of our average dMn_T concentrations. Thus, if there is a biological component to this apparent drawdown signal, it is likely a surface scavenging process not an uptake feature.

In the complete profile of Station 3 (Figure 2), Mn speciation had almost no structure, and nearly all the Mn was in the form of Mn(III)-L complexes. This could reflect an abundance of strong Mn(III)-binding ligands, stabilizing Mn(III) against oxidation to Mn(IV), and/or that dMn_T is well in excess of the biological assimilation requirement resulting in no uptake feature in the Chl-*a* maximum, and/or that there is an absence

Table 2
Physicochemical Data Collected From the CTD Rosette Package and Mn Speciation (in nM) Collected During the Diel Sampling at Station 2.

Depth	Time (EST)	Temperature (°C)	Florescence (mg m^{-3})	PAR	% Beam transmission	Salinity (ppt)	O_2 (μM)	Mn(II)	dMn(T)	Mn (III)-L	% Mn (III)-L	MnO_x
Surface	6:00	24.27	0.22	3.3	84.0	31.43	225.9	0.93 ± 0.95	52.35 ± 7.32	51.43 ± 7.38	98.23	0.16
	10:30	24.23	0.19	141.1	84.0	31.39	226.8	6.16 ± 2.41	130.82 ± 5.82	124.66 ± 6.30	95.29	0.08
	14:00	25.03	0.26	704.3	82.4	31.46	225.9	4.46 ± 0.95	5.00 ± 2.09	0.55 ± 2.30	10.93	0.08
	18:00	24.74	0.25	58.4	83.4	31.45	224.7	11.47 ± 1.96	28.85 ± 4.92	17.39 ± 5.30	60.25	0.16
	22:00	24.81	0.27	1.6	83.2	31.48	222.5	37.58 ± 0.43	76.15 ± 1.42	38.57 ± 1.49	50.65	0.16
Aphotic 1	6:00	9.76	0.39	ND	81.3	32.64	206.2	7.74 ± 1.80	39.31 ± 3.02	31.57 ± 3.52	80.31	2.76
	10:30	9.68	0.34	6.3	81.0	32.65	204.4	17.63 ± 0.30	88.54 ± 1.63	70.91 ± 1.66	80.09	3.23
	14:00	9.68	0.36	14.2	81.1	32.65	204.8	7.40 ± 1.99	46.58 ± 6.49	39.17 ± 6.79	84.10	2.97
	18:00	9.50	0.33	0.5	81.5	32.65	202.6	7.91 ± 5.23	4.22 ± 4.26	0.00 ± 6.75	0.00	3.68
	22:00	9.35	0.32	ND	81.4	32.67	203.3	38.33 ± 2.43	71.28 ± 3.74	32.94 ± 4.46	46.22	4.26
Aphotic 2	6:00	9.68	0.35	ND	81.6	32.65	204.9	14.18 ± 1.70	41.11 ± 3.39	26.93 ± 3.80	65.51	5.53
	10:30	9.64	0.32	2.0	80.8	32.64	203.3	12.74 ± 2.29	71.21 ± 3.02	58.47 ± 3.79	82.10	3.67
	14:00	9.68	0.34	9.1	81.6	32.65	204.0	1.19 ± 1.03	36.48 ± 2.15	35.29 ± 2.38	96.73	3.41
	18:00	9.50	0.36	0.1	81.5	32.64	201.9	4.73 ± 4.50	5.04 ± 4.25	0.31 ± 6.19	6.16	3.42
	22:00	9.35	0.28	ND	81.4	32.67	200.6	32.92 ± 2.39	53.47 ± 13.01	20.55 ± 13.23	38.43	4.45

Note. ND reflects values below the detection limit.

of reactive particles so scavenging reactions are less important at this site. However, these interpretations become convoluted when taking into consideration what we observe during a complete diel cycle at this site (section 4.2), as the soluble Mn speciation is highly variable in all three of our sampling depths at each of our five timepoints.

Lastly, an influence of lateral mixing on Mn speciation is best seen by comparing Station 1 to our other three stations. At well-mixed Station 1 we observe low concentrations of Mn oxides, which suggests slow oxidation relative to mixing but comparatively high stabilization of Mn(III)-L throughout the water column (aside from low % Mn(III)-L at 10-m depth). This may indicate that at well-mixed sites, Mn(III)-L complexes can accumulate as they are not being oxidized to Mn(IV) oxides, so the rate of formation MnO_x may be slower than the rate of mixing and/or there are inputs of Mn(III)-L via lateral mixing (such as terrestrial inputs, described above). However, as the only feature we see in the dissolved Mn speciation occurs at the top of the chlorophyll maximum at Station 1, and at the surface, we suggest that light-induced and biological processes govern the redox cycling at this site. The influence of mixing can also be seen in our diel cycle from Station 3 (see section 4.2).

4.2. Temporal Variability in Mn Speciation

We observe tremendous shifts in Mn speciation during our diel cycle (Table 2, Figure 3), emphasizing the importance of temporal variability in Mn speciation over short time scales at one site—on the order of hours. Because we have no lateral data at our study site, it is difficult to discern whether the dramatic shifts in total Mn over a diel cycle are the result of redox cycling or simply mixing processes. However, the 100-nM shift in dissolved Mn concentrations over the course of a diel cycle cannot be explained by corresponding changes in particulate Mn, thus pointing to lateral mixing as the dominant control on the variability we observe over the

course of a diel cycle. Though our hydrographic data seem to indicate that the water column has not mixed significantly, we can only assess vertical mixing processes and cannot account for lateral mixing. Thus, we can only propose possible redox mechanisms for the trends we observe but highlight that physical process is almost certainly also at play in this system. Regardless, these data reveal that taking one profile at one site at one timepoint is not sufficient for describing the redox speciation and concentration of a redox-sensitive element like Mn in dynamic coastal systems.

As observed in the depth profiles at each station (section 4.1), light and time of day have a dominant influence on the speciation of Mn. During the diel cycle examination at Station 3, dissolved Mn concentrations increase by 30 nM in bottom waters and 80 nM in surface waters at the onset of light in our second timepoint, which likely reflects some photo-reductive processes. However, we note that the pool of MnOx is an order of magnitude smaller than the dissolved Mn pool, thus either the cycling of solid-phase MnOx is faster than our sampling interval, or lateral mixing processes are a dominant control on the Mn profiles here. It is particularly interesting to see that MnO_X decreases from 3 nM to nondetectable at Aphotic 1 at the appearance of less than 1% surface irradiance, because significant light penetration and subsequent photo-induced reactions are not expected at this depth. While this low light level may have been sufficient to allow for photo-reductive dissolution of Mn oxides, the change in MnOx concentration is more likely due to mixing processes. By 14:00 EST, there is a decrease in dissolved Mn, and a slight increase in MnO_X, which could be the result of direct (i.e., enzymatic) and/or indirect (i.e., superoxide mediated) microbial Mn oxidation. This decrease is surprising given higher PAR at 14:00 than at 10:30, which we would expect to lead to more dissolved Mn. However, as total Mn (solid + soluble) decreases overall, this feature could also be the result of biological uptake (though we do not see a dramatic increase in fluorescence), or scavenging, as we do observe a decrease in beam transmission in surface waters, which could indicate high particulate matter. In the evening (18:00 EST) as PAR decreases in both aphotic depths, the concentration of dissolved Mn reached a minimum, which may correspond to oxidative removal processes as MnO_X concentrations increased slightly at this time. The rate of microbial Mn oxidation ranges from 0.4 to 3.5 nM/hr (Shiller & Stephens, 2005; Sunda & Huntsman, 1987), which means that this mechanism could only account for a 1.6–14 nM change in soluble Mn, less than 20% of our observed decrease at all depths, but could account for our total increase in MnO_X, which ranges from 0.2 to 4 nM, though mixing processes are also likely at play as mentioned below. The increase in MnO_x continues into our final timepoint, at 22:00 EST, indicating that these particles can accumulate in the absence of photo-reductive processes. Further, soluble Mn increased significantly at all depths in this time interval.

The variability in Mn speciation over a diel cycle observed here is not altogether surprising, given the known impacts of light and time of day on the circadian activity of organisms and chemistry of marine waters. Diel oscillations in the activity of light-dependent microorganisms, including cyanobacteria and diatoms, have been shown for both laboratory cultures and natural populations (e.g., Winter et al., 2004; Galí et al., 2013). More recently, diel cycling in the transcriptional activity of heterotrophic (nonphototrophic) bacterioplankton has also been shown, where peak transcript abundance from some of the most numerically abundant populations (e.g., *Pelagibacter, Roseobacter*) occurred in mid-afternoon (Ottesen et al., 2014). While diel variation in the expression of genes involved in direct enzymatic Mn oxidation (e.g., MnxG) has not been previously explored, ROS concentrations undergo strong diurnal fluctuations (Rose et al., 2008; Zhang et al., 2016). In fact, peak superoxide concentrations have been shown to occur midday in both sunlit and dark waters (Zhang et al., 2016), coinciding with the Mn oxide dynamics observed here. However, as peak hydrogen peroxide concentrations are also known to occur when PAR is highest, there are complex implications of ROS cycling with Mn as hydrogen peroxide can reduce oxidized forms of Mn. Further, oscillations in diurnal migrations and metabolic activities for different groups of microbiota (see, for instance, Ottesen et al., 2014) will lead to changes in the overall chemistry of waters both in photic and aphotic regions that will also undoubtedly influence Mn cycling.

Although we can draw on some biological and chemical processes to interpret the diel Mn cycle, it is likely that lateral mixing processes strongly influence the redox profile of Mn at coastal sites. This is reflected in Figure 3, where variability in the depth of the salinity and dO_2 maxima likely reflects slight shifts in position during our sampling and/or lateral mixing. That being said, in the afternoon timepoints (14:00–22:00 EST), there is little evidence of mixing during our sampling, and thus biogeochemical processes may dominate in the afternoon.

5. Conclusion

This is the first dataset examining the complete speciation of manganese from nonestuarine coastal waters, and the first complete diel cycle of Mn speciation. Further, this data expands the previous studies revealing the stabilization of Mn(III)-L in oxic waters (Oldham, Mucci, et al., 2017; Oldham, Miller, et al., 2017; Oldham, Tebo, et al., 2017).

Examining the speciation of Mn is important for better understanding the redox capacity of marine waters, as O_2 and MnO_x are the strongest oxidants in the ocean (Luther, 2010). Less well understood is the role and oxidation capacity of intermediate species like Mn(III)-L complexes, which are thought to cycle more rapidly but could have equal (or greater) oxidation capacities compared to Mn oxides. In this study, we observe the stabilization of Mn(III)-L at four biogeochemically diverse coastal sites. Mn(III)-L comprised the majority of total Mn at all sites, indicating that although they may be intermediates, Mn(III)-L complexes are perhaps less transient than previously thought. Although there are no obvious correlations between physicochemical parameters in the water column and the speciation of Mn, we note that vertical stratification leads to greater accumulation of oxidized species and structure in the profiles of all three Mn species. These findings are in-line with previous observations that stable redoxclines are requisite for the accumulation of dissolved reactive Mn (presumably Mn(III)-L) within stratified marine basins and lakes (Dellwig et al., 2012). We further observe that Mn oxides are stabilized in the bottom waters of all our stations, indicating that oxidation processes are important below the photic zone and chlorophyll maximum. Additionally, we find high concentrations of dissolved Mn in surface waters, which could reflect some influence from terrestrial runoff, and also high concentrations in bottom waters, suggesting that sediment resuspension and estuarine mixing are important sources of Mn to these waters.

Finally, we observe significant heterogeneity in Mn speciation on temporal and spatial (geographic and depth) scales in this study. Because the physicochemical parameters of the water column during our diel cycle sampling are shifting over time, lateral mixing processes play a critical role in the vertical structure of Mn speciation and this changes on the time scale of hours. Thus, studies examining redox profiles in coastal systems should examine lateral as well as vertical gradients to better reconcile the processes that control element distributions. Although lateral mixing is a likely dominant control on the diel shifts we observed, we note that light-mediated reactions are also critical in coastal systems in transformations of organic matter, the accumulation of ROS, and in metal photo-reductive processes. Our depth profiles and diel cycle measurements suggest that light plays a role in the cycling of Mn, even at nondetectable PAR levels. We observed a change of over 100 nM in Mn concentration over the course of only a few hours, suggesting that the coastal redox cycle of Mn is even more dynamic than previously thought. As particulate Mn cannot account for such a significant change, this change must be due to lateral mixing of waters high in dissolved Mn, pointing to the need for lateral profiling as well as vertical profiling for dynamic redox elements like Mn within coastal systems. Future explorations should target the underpinning physical and biogeochemical processes controlling the spatial and temporal heterogeneity of Mn cycling, which is necessary in accurately describing the fluxes and cycling of Mn within the global ocean.

Acknowledgments
This work was funded by grants from the Chemical Oceanography program of the National Science Foundation (OCE-1355720 to CMH and CHL). Véronique Oldham thanks Woods Hole Oceanographic Institution for the receipt of the WHOI Postdoctoral Scholarship. Thanks also to Kevin Sutherland, Jen Karolweski, Gabriella Farfan, Kalina Grabb, Kaitlin Bowman, Alison Agather, and Lindsey Starr for the shipboard sampling assistance, as well as the captain and crew of the R/V Endeavor who made the sampling for this research possible. All data presented in the manuscript are available through the Biological and Chemical Oceanography Data Management Office (BCO-DMO) under Project 756930 at the following link (https://www.bco-dmo.org/project/756930).

References

Altmann, H. J. (1972). Determination of dissolved oxygen in water with leukoberbelin-blue I. *A quick Winkler method. Anal. Chem.*, *262*, 97–99.

Anderson, C. R., Johson, H. A., Caputo, N., Davis, R. E., Torpey, J. W., & Tebo, B. M. (2009). Mn(II) oxidation is catalyzed by heme peroxidases in *Aurantimonas manganoxydans* strains SI85-9A1 and *Erythrobacter* sp. Strain SD-21. *Applied and Environmental Microbiology*, *75*, 4130–4138.

Baral, D., Lume-Pereira, C., Janata, A., & Henglein, A. (1985). Chemistry of colloidal manganese dioxide. 2. Reaction with superoxide anion (O2-) and hydrogen peroxide (pulse radiolysis and stop flow studies). *The Journal of Physical Chemistry*, *89*, 5779–5783.

Boyle, E. A., Collier, R., Dengler, A. T., Edmond, J. M., Ng, A. C., & Stallard, R. F. (1974). On the chemical mass-balance in estuaries. *Geochimica et Cosmochimica Acta*, *38*, 1719–1728.

Bruland, K. W., & Franks, R. P. (1983). Mn, Ni, Cu, Zn, and Cd in the western North Atlantic. In C. S. Wong, et al. (Eds.), *Trace Metals in Sea Water*, *NATO Conference Series (IV Marine Sciences)* (Vol, 9). Boston, MA: Springer.

Dellwig, O., Schnetger, B., Brumsack, H. J., Grossart, H. P., & Umlauf, L. (2012). Dissolved reactive manganese at pelagic redoxclines (part II): Hydrodynamic conditions for accumulation. *Journal of Marine Systems*, *90*, 31–41.

Diaz, J., Hansel, C. M., Voelker, B. M., Mendes, C. M., Andeer, P. F., & Zhang, T. (2013). Widespread production of extracellular superoxide by marine heterotrophic bacteria. *Science*, *340*(6137), 1223–1226. https://doi.org/10.1126/science.1237331

Duckworth, O. W., & Sposito, G. (2005). Siderophore-manganese(III) interactions I. *Manganite dissolution promoted by desferrioxamine-B. Environ. Sci. Technol.*, *39*(16), 6045–6051. https://doi.org/10.1021/es050276c

Duckworth, O. W., & Sposito, G. (2007). Siderophore-promoted dissolution of synthetic and biogenic layer type Mn oxides. *Chemical Geology*, *242*, 497–508.
Eastman, K. W., & Church, T. M. (1984). Behavior of iron, manganese, phosphate and humic acid during mixing in a Delaware salt marsh creek. *Estuarine, Coastal and Shelf Science*, *18*, 447–458.
Galí, M., Simó, R., Vila-Costa, M., Ruiz-González, C., Gasol, J. M., & Matrai, P. (2013). Diel patterns of oceanic dimethylsulfide (DMS) cycling: Microbial and physical drivers. *Global Biogeochemical Cycles*, *27*, 620–636.
Geszvain, K., McCarthy, J. K., & Tebo, B. M. (2013). Elimination of manganese(II, III) oxidation in Pseudomonas putida GB-1 by a double knockout of two putative multicopper oxidase genes. *Applied and Environmental Microbiology*, *79*(1), 357–366. https://doi.org/10.1128/AEM.01850-12
Goldberg, E. D. (1954). Marine geochemistry. I. Chemical scavengers of the sea. *Journal of Geology*, *62*, 249–265.
Graham, W. F., Bender, M. L., & Klinkhammer, G. P. (1976). Manganese in Narragansett Bay. *Limnology and Oceanography*, *21*, 665–673.
Hansard, S. P., Easter, H. D., & Voelker, B. M. (2011). Rapid reaction of nanomolar Mn(II) with superoxide radical in seawater and simulated freshwater. *Environmental Science and Technology*, *45*, 2811–2817.
Hansel, C. M. (2017). Manganese in marine microbiology. In R. K. Poole (Ed.), *Advances in microbial physiology* (pp. 37–83). Oxford: Academic Press.
Hansel, C. M., Buchwald, C., Diaz, J. M., Ossolinski, J. E., Dyhrman, S. T., Van Mooy, B. A. S., & Polyviou, D. (2016). Dynamics of superoxide production by natural *Trichodesmium* colonies from the Sargasso Sea. *Limnology and Oceanography*, *61*, 1188–1200.
Hansel, C. M., & Learman, D. R. (2015). Geomicrobiology of manganese. In H. L. Ehrlich, D. K. Newman, & A. Kappler (Eds.), *Ehrlich's geomicrobiology* (Vol. 6th, pp. 401–452). New York, NY: CRC Press.
Hansel, C. M., Zeiner, C. A., Santelli, C. M., & Webb, S. M. (2012). Mn(II) oxidation linked to superoxide production during asexual reproduction in an Ascomycete fungi. *Proceedings of the National Academy of Sciences of the United States of America*, *109*(31), 12,621–12,625. https://doi.org/10.1073/pnas.1203885109
Johnson, H. A., & Tebo, B. M. (2008). In vitro studies indicate a quinone is involved in bacterial Mn(II) oxidation. *Archives of Microbiology*, *189*(1), 59–69. https://doi.org/10.1007/s00203-007-0293-y
Learman, D. R., & Hansel, C. M. (2014). Comparative proteomics of Mn(II)-oxidizing and non-oxidizing Roseobacter clade bacteria reveal an operative manganese transport system but minimal Mn(II)-induced expression of manganese oxidation and antioxidant enzymes. *Environmental Microbiology Reports*, *6*(5), 501–509. https://doi.org/10.1111/1758-2229.12164
Learman, D. R., Voelker, B. M., Madden, A. S., & Hansel, C. M. (2013). Constraints on superoxide mediated formation of manganese oxides. *Frontiers in Microbiological Chemistry*, *4*(262). https://doi.org/10.3389/fmicb.2013.00262
Learman, D. R., Voelker, B. M., Vazquez-Rodriguez, A. I., & Hansel, C. M. (2011). Formation of manganese oxides by bacterially generated superoxide. *Nature Geoscience*, *4*, 95–98.
Luther, G. W. III (2005). Manganese(II) oxidation and Mn(IV) reduction in the environment—Two one-electron transfer steps versus a single two-electron step. *Geomicrobiology Journal*, *22*, 195–203.
Luther, G. W. III (2010). The role of one- and two-electron transfer reactions in forming thermodynamically unstable intermediates as barriers in multi-electron redox reactions. *Aquatic Geochemistry*, *16*, 395–420.
Luther, G. W. III, Madison, A. S., Mucci, A., Sundby, B., & Oldham, V. E. (2015). A kinetic approach to assess the strengths of ligands bound to soluble Mn(III). *Marine Chemistry*, *173*, 93–99.
Madden, A. S., & Hochella, M. F. Jr. (2005). A test of geochemical reactivity as a function of mineral size: Manganese oxidation by hematite nanoparticles. *Geochimica et Cosmochimica Acta*, *73*, 6517–6530.
Madison, A. S., Tebo, B. M., & Luther, G. W. III (2011). Simultaneous determination of soluble manganese(III), manganese(II) and total manganese in natural (pore)waters. *Talanta*, *84*, 374–381.
Madison, A. S., Tebo, B. M., Mucci, A., Sundby, B., & Luther, G. W. III (2013). Abundant porewater Mn(III) is a major component of the sedimentary redox system. *Science*, *341*, 875–878.
Marshall, J. A., de Salas, M., Oda, T., & Hallegraeff, G. (2005). Superoxide production by marine microalgae. *Marine Biology*, *147*, 533–540.
Moore, R. M., Burton, J. D., Williams, J. B., & Young, M. L. (1979). The behavior of dissolved organic material, iron, and manganese in estuarine mixing. Geochim. *Cosmochimica Acta*, *43*, 919–926.
Morgan, J. J. (2005). Kinetics of reaction between O_2 and Mn(II) species in aqueous solutions. *Geochimica et Cosmochimica Acta*, *69*, 35–48.
Nico, P. S., Anastasio, C., & Zasoski, R. J. (2002). Rapid photo-oxidation of Mn(II) mediated by humic substances. *Geochimica et Cosmochimica Acta*, *66*, 4047–4056.
Oldham, V. E., Miller, M. T., Jensen, L. T., & Luther, G. W. (2017). Revisiting Mn and Fe removal in humic rich estuaries. *Geochimica et Cosmochimica Acta*, *209*, 267–283.
Oldham, V. E., Mucci, A., Tebo, B. M., & Luther, G. W. (2017). Soluble Mn(III)-L complexes are abundant in oxygenated waters and stabilized by humic ligands. *Geochimica et Cosmochimica Acta*, *199*, 238–246.
Oldham, V. E., Owings, S. M., Jones, M. R., Tebo, B. M., & Luther, G. W. III (2015). Evidence for the presence of strong Mn(III)-binding ligands in the water column. *Marine Chemistry*, *171*, 58–66.
Oldham, V. E., Tebo, B. M., Jones, M. R., & Luther, G. W. (2017). Oxidative and reductive processes contributing to manganese cycling at oxic-anoxic interfaces. *Marine Chemistry*, *195*, 122–128.
Ottesen, E. A., Young, C. R., Gifford, S. M., Eppley, J. M., Marin, R., Schuster, S. C., et al. (2014). Mutlispecies diel transcriptional oscillations in open ocean heterotrophic bacterial assemblages. *Science*, *343*, 207–212.
Parker, D. L., Takami, M., Mylene, L., Mozafarzadeh, R. V., McCarthy, J. K., & Tebo, B. M. (2007). Inter-relationships of MnO2 precipitation, siderophore–Mn(III) complex formation, siderophore degradation, and iron limitation in Mn(II)-oxidizing bacterial cultures. *Geochimica et Cosmochimica Acta*, *71*, 5672–5683.
Rose, A. L., Godrant, A., Furnas, M., & Waite, T. D. (2010). Dynamics of nonphotochemical superoxide production and decay in the Great Barrier Reef lagoon. *Limnology and Oceanography*, *55*(4), 1521–1536.
Rose, A. L.; Webb, E. A.; Waite, T. D.; Moffett, J. W. Measurement and implications of nonphotochemically generated superoxide in the equatorial Pacific Ocean. *Environmental Science & Technology* 2008, *42* (7), 2387−2393.
Schneider, R. J., Roe, K. L., Hansel, C. M., & Voelker, B. M. (2016). Species-level variability in extracellular production rates of reactive oxygen species by diatoms. *Frontiers in Chemistry*, *4*, 5.
Shiller, A. M., & Stephens, T. H. (2005). Microbial manganese oxidation in the lower Mississippi River: Methods and evidence. *Geomicrobiology Journal*, *22*(3–4) (2005)), 117–125.
Sholkovitz, E. E. (1978). The flocculation of dissolved Fe, Mn, Al, Cu, Ni, Co and Cd during estuarine mixing. *Science Letters*, *41*, 77–86.

Stone, A. T. (1987a). Reductive dissolution of manganese(III/IV) oxides by substituted phenols. *Environmental Science & Technology*, *21*(10), 979–988. https://doi.org/10.1021/es50001a011

Stone, A. T. (1987b). Microbial metabolites and the reductive dissolution of manganese oxides: Oxalate and pyruvate. *Geochimica et Cosmochimica Acta*, *51*, 919–925.

Stone, A. T., & Morgan, J. J. (1984). Reduction and dissolution of manganese(III) and manganese (IV) oxides by organics: 2. Survey of the reactivity of organics. *Environmental Science & Technology*, *18*(8), 617–624. https://doi.org/10.1021/es00126a010

Sunda, W. G., & Huntsman, S. A. (1987). Microbial oxidation of manganese in a North Carolina estuary. *Limnology and Oceanography*, *32*(3) (1987)), 552–564.

Sunda, W. G., & Huntsman, S. A. (1988). Effect of sunlight on redox cycles of manganese. *Deep Sea Research*, *35*, 1297–1317.

Sunda, W. G., Huntsman, S. A., & Harvey, G. R. (1983). Photoreduction of manganese oxides in seawater and its geochemical and biological implications. *Nature*, *301*, 234–236.

Sundby, B., Silverberg, N., & Chesselet, R. (1981). Pathways of manganese in an open estuarine system. *Geochimica et Cosmochimica Acta*, *45*, 293–307.

Tebo, B. M., Bargar, J. R., Clement, B. G., Dick, G. J., Murray, K. J., Parker, D., et al. (2004). Biogenic manganese oxides, properties and mechanisms of formation. *Annual Review of Earth and Planetary Sciences*, *32*, 287–328.

Trouwborst, R. E., Clement, B. G., Tebo, B. M., Glazer, B. T., & Luther, G. W. III (2006). Soluble Mn(III) in suboxic zones. *Science*, *313*, 1955–1957.

Webb, S. M., Dick, G. J., Bargar, J. R., & Tebo, B. M. (2005). Evidence for the presence of Mn(III) intermediates in the bacterial oxidation of Mn(II). *Proceedings of the National Academy of Sciences*, *102*(15), 5558–5563. https://doi.org/10.1073/pnas.0409119102

Wehrli, B. (1990). Redox reactions of metal ions at mineral surfaces. In W. Stumm (Ed.), *Aquatic chemical kinetics: Reaction rate processes in natural waters*, (pp. 311–336). New York: Wiley.

Winter, C., Herndl, G. J., & Weinbauer, M. G. (2004). Diel cycles in viral infection of bacterioplankton in the North Sea. *Aquatic Microbial Ecology*, *35*, 207–216.

Wuttig, K., Heller, M. I., & Croot, P. L. (2013). Pathways of superoxide (O2–) decay in the Eastern Tropical North Atlantic. *Environmental Science and Technology*, *47*, 10,249–10,256.

Yakushev, E., Pakhomova, S., Sørenson, K., & Skei, J. (2009). Importance of the different manganese species in the formation of water column redox zones: Observations and modeling. *Marine Chemistry*, *117*, 59–70.

Yeats, P. A., Sundby, B., & Bewers, J. M. (1979). Manganese recycling in coastal waters. *Marine Chemistry*, *8*, 43–55.

Zhang, T., Hansel, C. M., Voelker, B. M., & Lamborg, C. H. (2016). Extensive dark biological production of reactive oxygen species in brackish and freshwater ponds. *Environmental Science & Technology*, *50*(6), 2983–2993. https://doi.org/10.1021/acs.est.5b03906